**Article ID**: 1000-7032(2023)12-2136-13

# A Low-density Ce-singly Doped Borosilicate Glass for Novel Short Lifetime Scintillating Material

ZHANG Fangming[1,2], LI Ce[1,3], LI Jianwei[1], LIU Wenxing[1], FU Yueying[1], JI Junjie[1], ZHENG Tao[1,4], GUO Yanyan[1,4,5*]

(1. *School of Materials Science and Engineering, Changchun University of Science and Technology, Changchun* 130022, *China*;
2. *Hubei New Huaguang Information Material Co., LTD, Xiangyang* 441100, *China*;
3. *Southwest Institute of Technical Physics, Chengdu* 610041, *China*;
4. *Engineering Research Center of Optoelectronic Functional Materials, Ministry of Education, Changchun University of Science and Technology, Changchun* 130022, *China*;
5. *Photonics Laboratory, King Abdullah University of Science and Technology(KAUST), Thuwal* 23955-6900, *Saudi Arabia*)
* *Corresponding Author, E-mail: guoyanyan@cust.edu.cn*

**Abstract**: Borosilicate glass possess natural advantage using as a scintillating material for detection field. To enrich the application requirements, the $Ce^{3+}$ ions doped borosilicate glass scintillation material $60B_2O_3$-$6SiO_2$-$3Al_2O_3$-$5BaO$-$15Na_2O$-$10La_2O_3$-$1Sb_2O_3$ was prepared. The structure was discussed based on density and FT-IR spectra indicating that the $Ce^{3+}$ ions exist as network modifiers. The ultraviolet(UV) absorption boundary was lower than 400 nm and the optical band gap was shorted to 2.93 eV. All these factors are conducive to the luminescent properties of $Ce^{3+}$ ions. The best emission spectrum was obtained at 372 nm with a 306 nm pumping. The optical basicity was increased with the concentration of $Ce^{3+}$ ions(0.539 2-0.541 7), which resulted in a light red shift of emission spectra. The fluorescence lifetime was as short as 24.39 ns, which shows obvious advantages compared with other $Ce^{3+}$ ions doped scintillation glass. These results provided a new material choice for the development of the detection field.

**Key words**: borosilicate glass; $Ce^{3+}$ doped; optical performance
**CLC number**: O482.31 **Document code**: A **DOI**: 10.37188/CJL.20230209

# 新型低密度短寿命铈单掺硼硅酸盐玻璃闪烁材料

张芳铭[1,2], 李 策[1,3], 李建苇[1], 刘文星[1],
付悦滢[1], 季俊杰[1], 郑 涛[1,4], 郭艳艳[1,4,5*]

(1. 长春理工大学 材料科学与工程学院, 吉林 长春 130012;
2. 湖北新华光信息材料有限公司, 湖北 襄阳 441100; 3. 西南技术物理研究所, 四川 成都 610041;
4. 长春理工大学 光电功能材料教育部工程研究中心, 吉林 长春 130012;
5. 阿卜杜拉国王科技大学 光子学实验室, 沙特阿拉伯 图沃 23955-6900)

**摘要**: 硼硅酸盐玻璃在探测领域作为闪烁基质材料具有天然的优势。本研究基于应用需求制备了$Ce^{3+}$离子掺杂硼硅玻璃闪烁材料$60B_2O_3$-$6SiO_2$-$3Al_2O_3$-$5BaO$-$15Na_2O$-$10La_2O_3$-$1Sb_2O_3$。基于密度和FT-IR光谱对玻璃的结构进行了分析,结果表明加入的$Ce^{3+}$离子作为网络修饰体存在。吸收光谱显示该材料紫外吸收边均低于400 nm、光学带隙缩短至2.93 eV,这些因素都有利于提升$Ce^{3+}$离子在基质材料中的发光特性。采用306 nm泵

**收稿日期**: 2023-09-14; **修订日期**: 2023-10-22
**基金项目**: 吉林省自然科学基金(20200201560JC)
Supported by Jilin Natural Science Foundation(20200201560JC)

浦波长,该材料在 372 nm 处得到了最佳的发射光谱。光学碱度随着 $Ce^{3+}$ 离子浓度的增加而增加(0.539 2~0.541 7)的现象与发射光谱的红移结果相吻合。荧光寿命短至 24.39 ns,与其他 $Ce^{3+}$ 离子掺杂玻璃闪烁材料相比具有明显的优势。这些优势为检测领域提供了一种新的材料选择。

**关　键　词**: 硼硅酸盐玻璃; $Ce^{3+}$ 掺杂; 光学性能

## 1　Introduction

With the rapid development of industrial exploration, high-energy physics research, medical imaging and other technologies, the demand for scintillation materials was continuing increasing and the hot of scintillation materials had last a long time[1-3]. Scintillation materials can emit UV or visible light under the radiation of X-ray, γ-ray and other high-energy particles[4-6]. It can conjunct with different photodetectors to realize the detection and analysis of high-energy rays or high-energy particles[7]. Scintillation crystals and scintillation glass were the most widely studied[8-9]. Although the scintillation glass was short of light yield compared with scintillation crystal, but its advantage of shorter decay time was also significant[10]. In addition, scintillation glass also had the advantages of simple preparation process, easy adjustment of components, low cost, high production efficiency, and large size materials, which is expected to become the preferred material to replace scintillation crystal in the civil field[1,8].

In the study of scintillation glass, $Ce^{3+}$ was the most popular activator and it had already been studied in several research[11-16]. Because $Ce^{3+}$ ($[Xe]4f^1$) had an allowed parity transition between 4f and 5d electronic configurations[17]. It had a strong absorption in the UV region and gave a strong and broad emission in visible range. The fast decays in the UV and visible range are about 20−50 ns[3,7,11,17-18]. Therefore, the interest of scintillation glass research was focused on the scintillation properties study of the $Ce^{3+}$ ions doped in different glass matrix[8,17-20]. Among all optical glasses, silicate glass had good thermal stability, low optical loss and greater advantages in strength and hardness because of the main composition of $SiO_2$[18-20]. However, the luminescence efficiency of doped rare earth ions was weakened by the high melting temperature of silicate glass[21]. The introduction of $B_2O_3$ in silicate glass will lower the melting temperature. It will also increase the refractive index, concentration of $Ce^{3+}$ ions and transmittance in the UV and visible range which will benefit the scintillation properties of $Ce^{3+}$ ions[22]. The most important effects of $B_2O_3$ are its high resistance to radiation and the possibility of scintillating in low density matrix[3,11]. And the scintillation materials prepared in this work were mainly used in the field of UV excitation, and lower density is conducive to excitation in the field of UV light. Therefore, the choice of borosilicate glass is more appropriate.

Based on the advantages of the borosilicate glass and the good scintillation properties of $Ce^{3+}$ ions, the physical and optical properties of $B_2O_3$-$SiO_2$-$Al_2O_3$-BaO-$Na_2O$-$La_2O_3$ (BSA-BNL) were chosen as the substrate. $Sb_2O_3$ was used as a reducing agent and $Ce^{3+}$ was introduced in the form of $CeO_2$. Firstly, the corresponding molar volume was calculated using the density of samples as well as the $Ce^{3+}$ ion concentration and ion spacing per unit volume were evaluated by molar volume. Secondly, the structure of the glass samples was investigated using FT-IR. Meanwhile, the UV-visible transmission spectra and fluorescence lifetimes were also tested. Finally, the relationship among fluorescence spectra, optical basicity and optical band gap was discussed to explore the application prospects of this scintillation material in the field of detection.

## 2　Experiment

### 2.1　Sample Preparation

This experiment was prepared by the melt quenching method with the chemical composition of $(60-x)B_2O_3$-$6SiO_2$-$3Al_2O_3$-5BaO-$15Na_2O$-$10La_2O_3$-$1Sb_2O_3$-$xCeO_2$ ($x$=0, 0.3, 0.4, 0.5, 0.6, 0.7), and

named C0-C5. Experiments were conducted in using high purity reagents ($H_3BO_3$ (99.9%), $SiO_2$ (99.9%), $Al_2O_3$(99.9%), $BaCO_3$(99.9%), $Na_2CO_3$ (99.9%), $La_2O_3$(99.9%), $Sb_2O_3$(99.9%), and $CeO_2$ (99.9%)). Among them, $Sb_2O_3$ was used to provide a reducing atmosphere. The raw materials of each sample are weighed (10 g), mixed, and ground. The powder was melted in a corundum crucible at 1 300 ℃ for 1 h. Then it was cast on an iron plate preheated at 200 ℃ and annealed at 50 ℃ for 2 h immediately. After that, it was cooled to room temperature at a rate of 1 ℃/min. The samples were cut and polished for physical and optical test. The shape of optical test samples was 10 mm×10 mm×2 mm. The powder samples were used for FT-IR spectra test.

### 2.2 Characterizations

The density of the glass samples was tested by Archimedes drainage method using an MD-2014 density tester at room temperature. Each glass sample was measured three times and averaged. Infrared absorption spectra were tested using a Fourier transform infrared spectroscopy manufactured by Perkin Elmer. Absorption and transmittance in UV and visible range were tested by a Perkin Elmer Lambda 950 in the range of 200-800 nm. Excitation and emission spectra were measured using a Shimadzu RF-5301PC type fluorescence spectrometer from Japan. Fluorescence lifetime was measured using a Fluo Time 300 fluorescence lifetime spectrometer. XPS spectra tests were performed using ThermoFisher Nexsa's XPS equipment.

## 3 Results and Discussion

### 3.1 Physical Properties

In this experiment, the physical properties of C0-C5 glass samples were listed in Tab. 1, which includes density ($\rho$), molar volume ($V_m$), ion concentration per unit volume of Ce ($N_i$), and average Ce-Ce inter-core distance ($r_i$). The values of $N_i$ and $r_i$ were calculated by $\rho$ and $V_m$, the specific values in Tab. 1 were obtained by Formulas (1) and (2)[23], where $C$ represents $CeO_2$ doping concentration:

$$N_i = \frac{C*NA}{V_m}, \tag{1}$$

$$r_i = \left(\frac{1}{N}\right)^{1/3}. \tag{2}$$

The trend of density, molar volume, ion concentration, and inter-core distance of C0-C5 glass samples (the value listed in Tab. 1) were plotted according to the increase of $CeO_2$ ions, as shown in Fig. 1. First, this borosilicate glass has low density compared with other scintillating materials[3,10]. It can be found that the density and molar volume of C0-C5 glass samples gradually increased gently with the increase of $CeO_2$ content. At the same time, $N_i$ of Ce

**Tab. 1 Relevant physical parameters of C0-C5 glass samples**

| Number | $\rho$/ ($g\cdot cm^{-3}$) | $V_m$/ ($cm^3\cdot mol^{-1}$) | $N_i$/ ($10^{19}\,cm^{-3}$) | $r_i$/ ($10^{-10}$ m) |
|---|---|---|---|---|
| C0 | 2.986 | 33.784 | — | — |
| C1 | 3.010 | 34.536 | 5.231 | 2.674 |
| C2 | 3.015 | 34.819 | 6.918 | 2.436 |
| C3 | 3.025 | 35.042 | 8.592 | 2.266 |
| C4 | 3.028 | 35.356 | 10.219 | 2.138 |
| C5 | 3.048 | 35.455 | 11.889 | 2.034 |

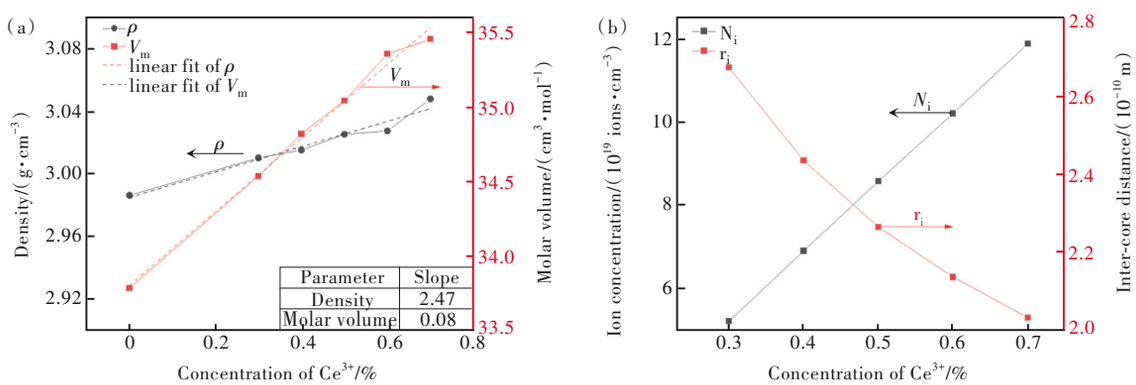


Fig.1 (a) Density ($\rho$) and molar volume ($V_m$) trends of glass samples, inset table shows the linear fit slope of density and molar volume. (b) Ion concentration ($N_i$) and inter-core distance ($r_i$) trends of glass samples

increases continuously with the increase of $CeO_2$ content, as well as the $r_i$ decreases continuously. The change in density can be attributed to the increased $CeO_2$ by replacing $B_2O_3$ of the glass component, which has larger relative molecular mass of $CeO_2$ (172.11 g/mol) compared with that of $B_2O_3$ (69.62 g/mol). Additionally, based on the Pauling's rules in crystal chemistry for the ionic structure architecture the $Ce^{3+}$ should be six-coordinated by $O^{2-}$ ($R_{Ce^{3+}}/R_{O^{2-}}$=0.649<0.732)[24]. In other words, the introduced $Ce^{3+}$ ions will enter the network gap but not destroy the glass network structure. It also gave a possibility of increased density obviously (2.07%), which exceed the change of $CeO_2$ concentration (0.7%). Considering the error, the range of density change indicates that the influence of introduced $CeO_2$ on glass structure is mild. And it can be also observed from Fig. 1 that the molar volume also rises slightly (4.95%) which can be ascribed to the increased $CeO_2$. As we all know that the $Ce^{3+}$ ions have larger atomic number ($Z$=58) and the $Ce^{3+}$ ions enter the space of network, thus the introduced $CeO_2$ will lead to an increase in density. The molar volume and the density are proportionally increased. But the slope of density is larger than the molar volume. It predicts a slightly loose glass structure, likely due to the introduced $CeO_2$. This phenomenon can be identified by the FT-IR spectra.

In the borosilicate glass system, $CeO_2$ exists as network modifier and the Ce—O bond has strong ionicity and the oxygen ion is easy to be separated from the cation[24]. It was a free oxygen provider. Secondly, because of the large ionic radius of $Ce^{3+}$ ions the introduced $Ce^{3+}$ ions will also play the role of breaking the network. Meanwhile, the increase of $CeO_2$ content will decrease the optical band gap which can be confirmed by the changed absorption band[25]. The smallest $r_i$ is about 0.2 nm, which is larger than the cation radius of $Ce^{3+}$ (0.091 nm), predicting an enhanced spectra properties and less probability of cluster.

### 3.2 XRD Spectra

XRD is an important means to analyze the crystal field structure in the study of amorphous glass materials. In our work, the peaks of C0-C5 glass samples in XRD tests were basically the same. Combined with the analysis of emission spectra in 3.7 part, the C4 glass sample has the highest luminous intensity. Therefore, XRD spectrum of C4 glass sample was selected for analysis (as shown in Fig. 2). As can be seen from the Fig. 2, there was "steamed bun peak" and no sharp objects were found. It showed obvious amorphous characteristics, which confirm the existence of amorphous properties and long-range structure disorder in the glass. The borosilicate glass system doped with $CeO_2$ showed an ideal glassy state.

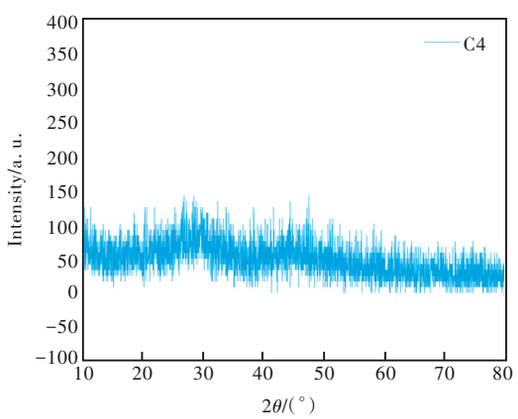


Fig.2　XRD spectrum of C4 glass sample

### 3.3 FT-IR Spectra

The network structure of the glass samples was investigated using FT-IR. The composition of $CeO_2$ was the mainly change in our work which exists as a network modifier and has less effect on the network structure in the glass samples. So, the infrared absorption spectra of C0 and C4 glass samples were selected for comparative analysis as shown in Fig. 3 (a) and (b) were the infrared absorption spectra of C0 glass sample ($C_{CeO_2}$=0%) and C4 glass sample ($C_{CeO_2}$=0.6%), respectively.

From Fig. 3 we can found that both C0 and C4 glass samples contain nine absorption peaks labeled in the figure. The vibration corresponding to each peak was listed in Tab. 2. All peaks in Fig. 3 had been normalizing using Gaussian fitting to distinguish position of the peaks. Based on the comparation of Fig. 3 (a) and (b), it was found that the peak position of the glass has no obvious change, indicating

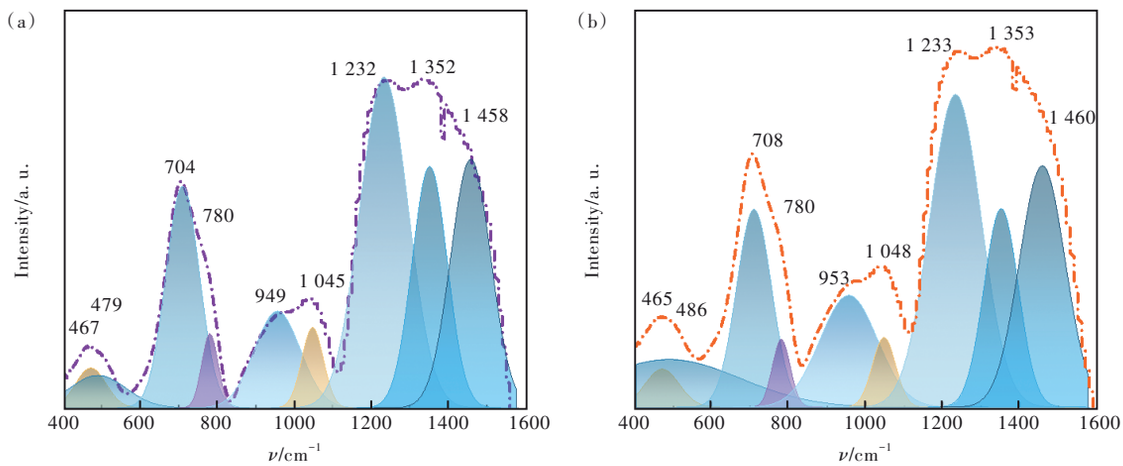


Fig.3 (a)Infrared absorption spectra of C0 glass sample. (b)Infrared absorption spectra of C4 glass sample.

**Tab. 2 FT-IR absorption peaks of C4 glass samples and the corresponding vibrational modes**

| Wavenumber/cm$^{-1}$ | Vibration mode |
|---|---|
| 400–470 | Bending vibration of Si—O—Si, Si—O—Al[26] |
| 470–600 | In-plane bending vibration of the [$BO_3$] unit[27] |
| 680–720 | Bending vibration of the B—O—B bonds of the [$BO_3$] unit[28] |
| 750–800 | Bending vibration of the Al—O bond in the [$AlO_4$] unit[26-27] |
| 900–1 000 | Stretching vibration of the B—O bond in the [$BO_4$] unit[29] |
| 1 020–1 100 | Asymmetric stretching vibration of Si—O—Si[27] |
| 1 200–1 300 | Stretching vibration of the B—O bond in the [$BO_3$] unit[26,30] |
| 1 300–1 400 | Asymmetric stretching vibration of the B—O bond in the [$BO_3$] unit[26,28] |
| 1 420–1 550 | B—$O^-$ vibrations in borate networks[31] |

that the addition of $CeO_2$ has no obvious influence on the network structure of borosilicate glass. It can be concluded that the main structures in this borosilicate glass were [$BO_3$], [$BO_4$] and [$SiO_4$] units[26-29]. The introduced $CeO_2$ did not generate new detectable vibrations in the samples. One of the reasons that $CeO_2$ exists as a network modifier in the samples. The other reason is low concentration of introduced $CeO_2$ in all samples. These results were consistent with the above inferences about $\rho$, $V_m$, $N_i$ and $r_i$.

### 3.4 XPS Spectra

XPS tests were performed to investigate the oxidation distribution of Ce and the attribution of fluorescence emission. Combined with the analysis of photoluminescence spectra in the following 3.7 part, C4 samples were selected for XPS spectra analysis of complex Ce 3d, and the results were shown in Fig. 4.

Among them, Fig. 4(a) showed the main elements contained in the C4 sample and valence states. In all samples, Ce exists in the form of $Ce^{3+}$ and $Ce^{4+}$ oxidation states. In order to further explore the relative concentrations of $Ce^{3+}/Ce^{4+}$, a local magnification diagram was drawn(as shown in Fig. 4 (b)). It can be seen from Fig. 4(b) that the binding energies corresponding to $Ce^{4+}$ and $Ce^{3+}$ are 886.7 eV and 903.7 eV, respectively[32-33].

The relative concentration of $Ce^{3+/4+}$ and ($Ce^{3+}$+$Ce^{4+}$) in Ce ions can be calculated by the ratio of the peak area ($ACe^{3+/4+}$) to all the peak areas ($ACe^{3+}$+$ACe^{4+}$)[34]. From the analysis of fitting results in Tab. 3, it can be calculated that the relative concentration of $Ce^{3+}/Ce^{4+}$ in C4 sample is 1.283. It can be shown that Ce in the sample mainly exists in the form of $Ce^{3+}$. Combined with the emission spectra analysis in 3.7 part, it was further demonstrated that $Ce^{3+}$ is the main ion of fluorescence luminescence.

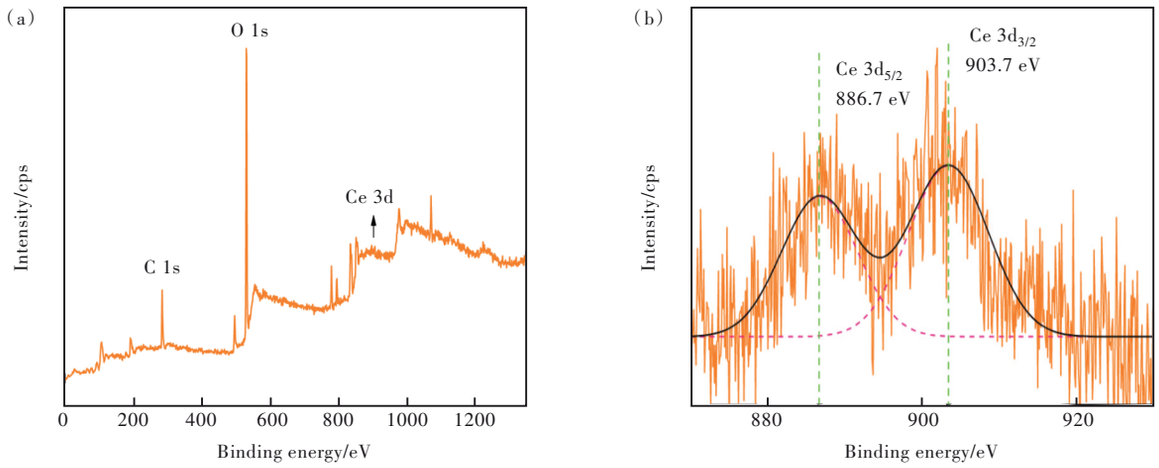


Fig.4　(a)XPS spectrum of C4 glass samples. (b)Locally enlarged image(Ce 3d).

**Tab. 3　Ce 3d track XPS test fitting results**

| Ion species | Binding energy/eV | Peak area($A$) |
|---|---|---|
| Ce $3d_{5/2}$($Ce^{4+}$) | 886.7 | 6 547.65 |
| Ce $3d_{3/2}$($Ce^{3+}$) | 903.7 | 8 396.58 |

### 3.5　Transmission Spectra

The UV-Vis transmission spectra of C0–C5 glass samples with different $CeO_2$ contents were shown in Fig. 5(a). The inset figure of Fig. 5(a) is the photo of annealed glass of C4 sample. It was clear that all the samples had good transmission (above 75%). A broad absorption band can be observed in Fig. 5(a), which is due to the electronic transition of the 4f-5d orbital of $Ce^{3+}$. With the increase of $CeO_2$, there were a clear red-shift of the UV absorption edge. To illustrate it the UV absorption edge part of Fig. 5(a) were enlarged in Fig. 5(b). The UV absorption edge of matrix glass (C0) is 320 nm. While that of C1–C5 samples was 331, 343, 347, 349, 353 nm, respectively. All of them were less than 400 nm which can effectively reduce the generation of self-absorption and is beneficial to the sensitivity of high-energy ray or high-energy particle detection. It was known that the absorption band of $Ce^{4+}$ ions is caused by the charge transfer state from $O^{2-}$ to $Ce^{4+}$. The charge transfer band of $Ce^{4+}$ ions in oxide glasses was wider than that of $Ce^{3+}$ ions. It can be extended from the far-UV region to the visible region, even up to about 500 nm[35]. With the increase of $CeO_2$, the concentration of $Ce^{4+}$ ions will be increased gradually. It will cause a red shift in the samples[36]. Additionally, the increased $CeO_2$ will enlarge the crystal field strength of the glass network structure. Then the energy gap between the 5d and 4f orbits of $Ce^{3+}$ became smaller and it made an easier electrons transition between the 4f and 5d

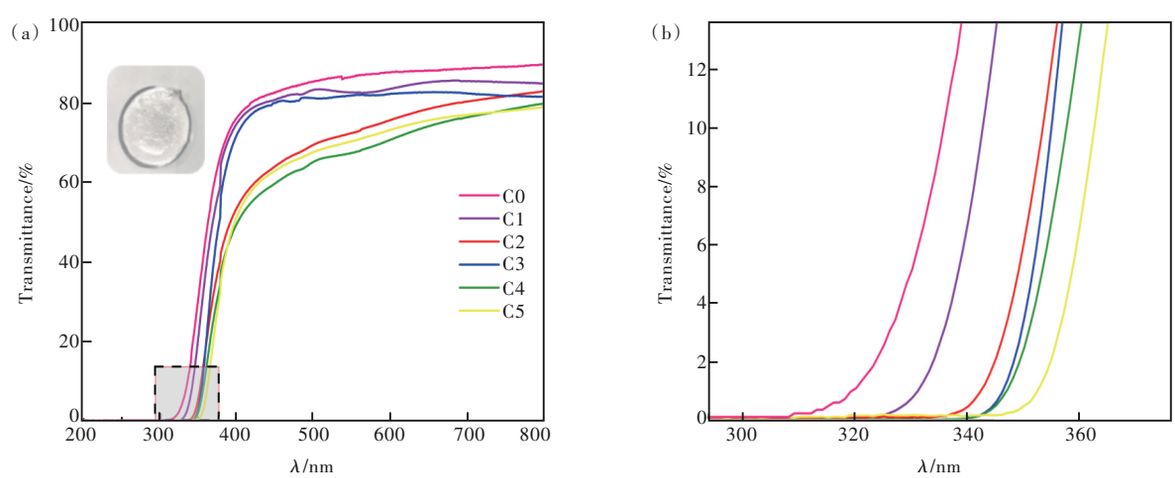


Fig.5　(a)UV-Vis's transmission spectra of C0–C5 glass samples(Inset: diagram of annealed C4 sample). (b)Local enlarged view.

orbits[37]. It also predicts an increased emission spectrum.

### 3.6 Optical Band Gap

Optical band gap ($E_g$) is an important parameter for predicting the electronic states of crystalline and amorphous solids. The level of $E_g$ can characterize the size of the band gap of materials, which values the possibility of material as a luminescent host material. The $E_g$ value can be calculated by the expression derived independently by Tauc and Mott-Davis[38]. The expression is shown in Formula (3):

$$(\alpha h\nu)^m = B\left(h\nu - E_g\right), \tag{3}$$

where $\alpha$ is the absorption coefficient, $h$ is the plank constant, $\nu$ is the frequency of the incident photon and the parameter $B$ is the trailing parameter, calculated from the slope of $(\alpha h\nu)$ relative to $(h\nu - E_g)$. $m$ is an exponential value describing the transition type, which is allowed indirectly when $m$=1/2; when $m$=1/3, it means indirect prohibition; when $m$=2, indicates direct permission; when $m$=3, it means direct prohibition. In this experiment, the prepared glass sample is an amorphous solid, which should be selected indirectly, corresponding to $m$ =1/2. The optical band gap of C0-C5 glass samples was calculated and plotted by absorption spectroscopy. The indirect band gap was represented by $(\alpha h\nu)^{1/2}$, as shown in Fig. 6. The specific optical band gap $E_g$ values were listed in Tab. 4.

Combining the specific values of $E_g$ in Tab. 4 with the variation trend in Fig. 6, it can be obtained that the indirect band gap of C0-C5 glass samples

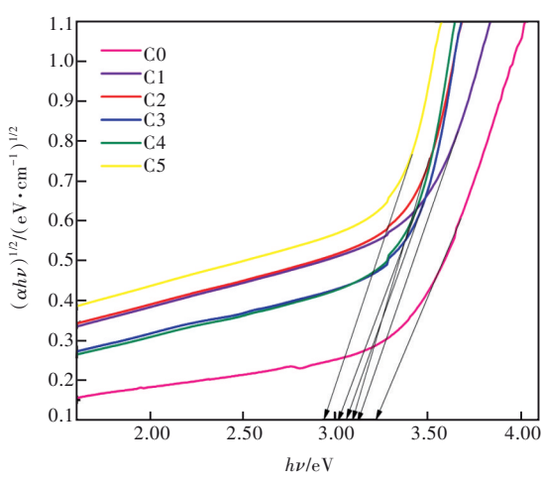


Fig.6 Optical band gap values of C0-C5 glass samples

Tab. 4 Optical band gap values of C0-C5 glass samples

| Number | $E_g$/eV |
|---|---|
| C0 | 3.22 |
| C1 | 3.12 |
| C2 | 3.08 |
| C3 | 3.05 |
| C4 | 3.01 |
| C5 | 2.93 |

gradually decreases from 3.22 eV to 2.93 eV with the increase of $CeO_2$ content. It was beneficial to the emission of $CeO_2$[39].

Additionally, we all know that the decrease of the optical band gap means an increase in the number of non-bridging oxygen[40]. The increase in the amount of non-bridging oxygen leads to an increase in the negative load around the Ce ion, thus improving the optical basicity. The bonding strength of non-bridged oxygen is less than that of bridged oxygen with excited electrons, which results in less transition energy through optical band gap. In addition, since the optical band gap of the glass system decreases with the increase of the average atomic number, the atomic number of $Ce^{3+}$ is higher than that of $B^{3+}$, and the outermost electrons of $Ce^{3+}$ are more active and less bound than those of $B^{3+}$, thus making the glass system more active and more beneficial to the occurrence of optical band gap transition.

But the FT-IR spectra did not show an obvious change on the spectra of non-bridging oxygen. In our opinion, these results can be ascribed to the low concentration of $CeO_2$. And the introduced $CeO_2$ will provide free oxygen. So, the values of $E_g$ were decreased by the increase of $CeO_2$.

### 3.7 Photoluminescence Spectra

The excitation and emission spectra of the glass samples were tested and the spectra of C4 sample with 0.6% doped $CeO_2$ were selected for showing in Fig. 7 for example. The excitation spectra of $Ce^{3+}$ was composed of an asymmetric broadband. At the measuring wavelength of 370 nm, the maximum excitation spectra were 306 nm corresponding to the 4f→5d transition of $Ce^{3+}$. A strong broadband luminescence of $Ce^{3+}$ was also shown in the emission spectra corresponding to the transition from 5d state to 4f

ground state under 306 nm UV excitation. The maximum emission wavelength was about 370 nm, and the Stokes shift was 64 nm. It can be evaluated that the $Ce^{3+}$ in our samples has a [Xe] $4f^1$ electronic configuration with a large full width of half maximum (FWHM) of emission peak(about 68.28 nm). It indicated that environment of the crystal field has a significant effect on the electronic configuration of the $Ce^{3+}$ 5d energy level. It resulted to a relatively wide energy level splitting. So, the emission spectra of $Ce^{3+}$ can be observed to be non-uniform broadening from Fig. 7.

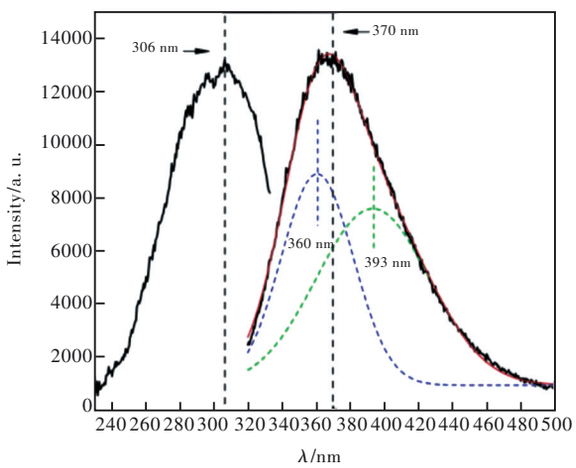


Fig.7　Excitation and emission spectra of C4 glass sample

The nonlinear curve fitting of emission spectra is carried out by Gauss model. It can be observed that the emission of $Ce^{3+}$ came from two transitions, namely $^5D_{3/2}\rightarrow{}^2F_{5/2}$ transition and $^5D_{3/2}\rightarrow{}^2F_{7/2}$ transition, respectively. They can be ascribed to the corresponding emission peaks at 360 nm and 393 nm, respectively[21]. The ground state of the $Ce^{3+}$ ion is a doublet ($^2F_{5/2}$ and $^2F_{7/2}$) as diagrammatically shown in Fig. 8. The double characteristics of the emission bands may be due to the lack of specific symmetries or long-range periodicity in the glass, causing the active ions to experience a random distribution of local fields. This results in a large random variation in the position occupied by a single 4f ion, which is also one of the reasons for the uneven broadening of the emission spectra of $Ce^{3+}$.

To evaluate the effect on emission spectra caused by the increased $CeO_2$, the emission spectra of C1−C5 glass samples were shown in Fig. 9 with an

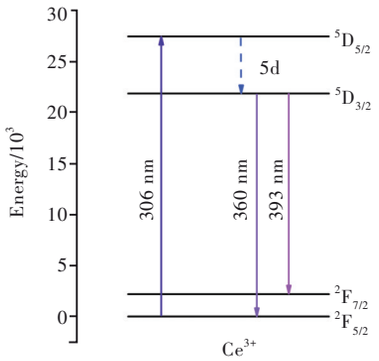


Fig.8　$Ce^{3+}$ energy level transition diagram

excitation wavelength at 306 nm. The dotted line in the upper right corner of Fig. 9 showed the change of luminescence intensity with $CeO_2$ content. It can be observed that the luminescence intensity gradually increases with the increase of $CeO_2$ content until the concentration of $CeO_2$ is 0.6%(C4). When the doping concentration of $CeO_2$ is 0.6%(C4), the luminescence intensity was the highest. When the content of $CeO_2$ continued to increase, the luminescence intensity was decreased. There are two main reasons. Firstly, with the increase of $CeO_2$ content the concentration of $Ce^{4+}$ and $Ce^{3+}$ ions increased at the same time with the constant concentration of $Sb_2O_3$. The content of $Sb_2O_3$ is certain in our sample. With the continuous increase of $CeO_2$ content, $Sb_2O_3$ cannot satisfy the need for reducibility. More $CeO_2$ will be exist in the form of $Ce^{4+}$ ions with non-luminescent. As we all know that the exist of $Ce^{4+}$ ions were harm to the emission of $Ce^{3+}$ ions[35]. So, the emission of $CeO_2$ doped glass sample will not vary linearly with the increase of $CeO_2$. It can be identified by the inner figure of Fig. 9. Secondly, according to the principle of interaction between electric dipoles, the cross-relaxation probability is inversely proportional to the distance between adjacent activated ions. According to the study of Ce ion concentration and Ce-Ce ion spacing in unit volume in 3.1 part, it can be found that when the content of $CeO_2$ increased gradually, the concentration of Ce ions in unit volume was increased gradually. The distance between adjacent Ce ions was decreased resulting a stronger effect on $Ce^{3+}$ ions by $Ce^{4+}$ ions. Therefore, the best concentration of $CeO_2$ in this borosilicate

glass was 0.6%.

It can also be observed from Fig. 9 that the emission peak center was in the range of 354–378 nm, which is mainly caused by the 5d→4f transition of $Ce^{3+}$ ions. The emission peak showed an obvious red shift. Combined with the analysis of the optical band gap in 3.6 part, the non-bridged oxygen will provide negative charges which were located between the inner core of $Ce^{3+}$ and the 4f orbit. These gap negative charges can shield the electrostatic attraction between the nucleus and the 4f orbit and short the energy gap of 4f-5d. Therefore, with the increase of $CeO_2$ content, the emission spectra of $Ce^{3+}$ under the 5d→4f transition gradually releases photons with longer wavelengths[41].

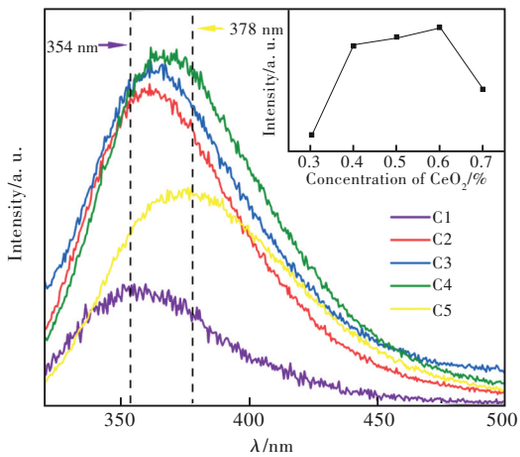


Fig.9 Emission spectra of C1–C5 glass samples

In addition, the change of optical basicity is also one of the important factors affecting the red shift of emission spectra[40,42-43]. The optical basicity of glass refers to the ability of oxygen atoms to contribute electrons, which is a characterization method of the electron cloud expansion effect. It can reflect its optical properties and chemical structure. The calculation of the theoretical optical basicity can be obtained by the following Formula (4)[43]:

$$A_{\mathrm{th}}=\frac{\frac{1}{2}aN_A\Lambda\left(AO_{\frac{a}{2}}\right)+\frac{1}{2}bN_B\Lambda\left(BO_{\frac{b}{2}}\right)+\cdots+cN_C\Lambda(CF_c)+dN_D\Lambda(DF_d)+\cdots}{\frac{1}{2}aN_A+\frac{1}{2}bN_B+\cdots cN_C+dN_D+\cdots},\tag{4}$$

among them, $AO_{a/2}$ and $BO_{b/2}$ represent single oxides, $CF_c$ and $DF_d$ represent fluorides; $a$, $b$, $c$, $d$ are the charge of cation $A$, $B$, $C$, $D$ respectively; $N_A$, $N_B$, $N_C$, $N_D$ represent molar ratios. The parameter $\gamma$ and the single oxide alkalinity $\Lambda$ were adjusted and the electronegativity $\chi$ of the element $A$ was estimated using the following Formula (5):

$$\frac{1}{\Lambda\left(AO_{\frac{a}{2}}\right)}=\gamma\left(AO_{\frac{a}{2}}\right)=1.36(\chi-0.26),\tag{5}$$

the electronegativity of B, Si, Al, Ba, Na, Sb, Ce and La are 2.04, 1.9, 1.61, 0.89, 0.93, 2.05, 1.12 and 1.1, respectively. It can be seen from Fig. 10 that the optical basicity of C1–C5 glass samples varies linearly from 0.539 2 to 0.541 7 with the increase of $CeO_2$ contents, which is consistent with the trend of the optical basicity resulted by the increased non-bridge oxygen in 3.6 part. The increased optical basicity indicated that oxygen atoms possess a strong ability of giving electrons and a strong ionicity. It will short the energy gap of 4f-5d further. It will contribute to the red shift in the emission spectra[44].

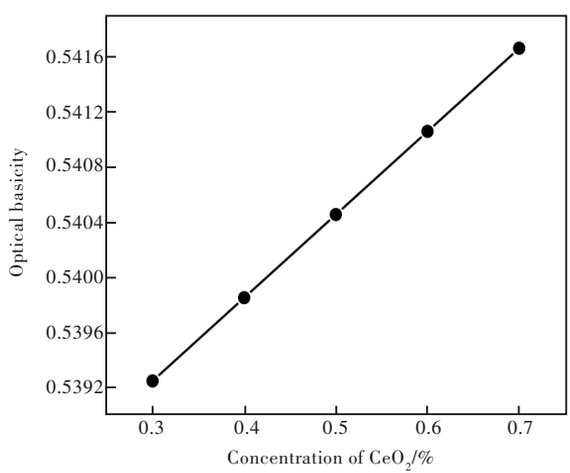


Fig.10 Variation trend of optical basicity under different $CeO_2$ contents

### 3.8 Fluorescence Lifetime

Fluorescence lifetime is one of the most important parameters to judge the scintillation properties of materials. In this experiment, the fluorescence lifetime of C1–C5 glass samples doped with different $CeO_2$ contents was tested and shown in Fig. 11. From the excitation spectra of Fig. 7, the excitation

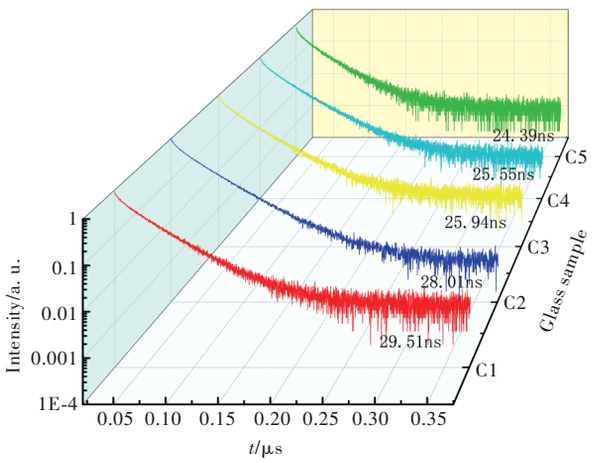


Fig.11　Fluorescence lifetime of C1–C5 glass samples

peak was located at 306 nm. Therefore, the closest 320 nm pumping source was selected as the excitation source to test the fluorescence lifetime of the emission peak at 370 nm. The attenuation curve can be well fitted by the double exponential function. The expression is shown in Formula (6):

$$I(t)=I_0+A_1\exp(-t/\tau_1)+A_2\exp(-t/\tau_2), \quad (6)$$

among them, $I_0$, $A_1$ and $A_2$ are represented as the fitting parameter values, $t$ is the time, $\tau_1$ and $\tau_2$ are expressed as the decay time of each exponential component. The very short decay time of $\tau_1$ belongs to the photon pulse of the diode laser source less than 2 ns, and $\tau_2$ corresponds to the fast luminescence of $Ce^{3+}$. The specific average decay time of the glass sample can be calculated by Formula (7):

$$\tau_{ave}=\left(A_1\tau_1^2+A_2\tau_2^2\right)/\left(A_1\tau_1+A_2\tau_2\right), \quad (7)$$

based on the above Formulas (6) and (7), the specific decay time parameters for C1–C5 glass samples in Tab. 5 can be obtained. The nanosecond scale shows that the 5d-4f transition of $Ce^{3+}$ has a very short fluorescence lifetime. It can be ascribed to the 5d-4f transition of $Ce^{3+}$ ions which is an allowed electric dipole transition. With the increase of $CeO_2$ content, the decay time of the glass sample gradually decreases. Considering the structural changes of our samples with the increase of $CeO_2$, the shorted lifetime can be ascribed to the decreased $r_i$ and increased optical basicity.

**Tab. 5　Decay time of each index component and the average decay time of C1–C5 glass samples**

| Number | $\tau_1$/ns | $\tau_2$/ns | $\tau_{ave}$/ns |
|---|---|---|---|
| C1 | 29.72 | 29.53 | 29.51 |
| C2 | 16.29 | 36.89 | 28.01 |
| C3 | 12.16 | 37.06 | 25.94 |
| C4 | 11.32 | 34.85 | 25.55 |
| C5 | 13.75 | 32.77 | 24.39 |

In Tab. 6, the relative literature on cerium-doped borosilicate glass is described in detail, in which the glass composition, decay time($\tau_1$, $\tau_2$, $\tau_{ave}$) and reference sources are described in detail. Compared with the decay time of C1–C5 glass sample ($\tau_1$, $\tau_2$, $\tau_{ave}$) in Tab. 5, it can be concluded that the glass sample prepared in this experiment has ultra short decay time.

Fig. 11 showed that the lifetime reached a relatively identical value in C3, C4 and C5 samples with the increase of the $CeO_2$ concentration. Combined with the analysis of excitation and emission spectra of glass samples in 3.7 part, the luminescence intensity of C4 glass samples is the strongest. Extra $CeO_2$ will decrease the luminescence intensity which will reduce its application value. In brief, this cerium doped borosilicate glass shows strong potential in high sensitivity detection.

**Tab. 6　Literature review on cerium-doped borosilicate glasses: glass composition, decay time and respective reference sources**

| Glass composition | $\tau_1$ | $\tau_2$ | $\tau_{ave}$ | Ref. |
|---|---|---|---|---|
| $47SiO_2$-$28B_2O_3$-$14Na_2O$-10.8MgO-0.1$CeO_2$-0.1($Sb_2O_3$/$SnO_2$/$P_2O_5$) | 36–40 ns | 145–259 ns | — | [45] |
| $20SiO_2$-(28–38)$B_2O_3$-$15BaF_2$-(10–20)$Lu_2O_3$-(10–20)$Gd_2O_3$-$2CeF_3$ | — | — | 33–41 ns | [46] |
| $25Gd_2O_3$-10CaO-$10SiO_2$-(55–$x$)$B_2O_3$-$xCeF_3$ | — | — | 36–49 ns | [47] |
| (30.5–$x$)$SiO_2$-$24B_2O_3$-$3BaCO_3$-$9Al_2O_3$-$30Gd_2O_3$-$3P_2O_5$-0.5$Sb_2O_3$-$xCe_2O_3$ | 45–90 ns | 0.9–4 μs | — | [7] |
| $15SiO_2$-$30B_2O_3$-$25Al_2O_3$-$30Gd_2O_3$+1 $CeO_2$(%) | 40 ns | 136 ns | — | [41] |

## 4 Conclusion

In this work, a series of $(60-x)B_2O_3$-$6SiO_2$-$3Al_2O_3$-$5BaO$-$15Na_2O$-$0La_2O_3$-$1Sb_2O_3$-$xCeO_2$ ($x$ = 0, 0.3, 0.4, 0.5, 0.6, 0.7) glass samples were prepared by melt quenching method. The physical and optical properties were studied.

Firstly, their physical properties were analyzed. It was found that the density and molar volume of the glass samples increased gradually with the increase of $CeO_2$ content. At the same time, the ion concentration of Ce in unit volume was also increased, which was negatively correlated with the Ce-Ce ion spacing. Secondly, the FT-IR spectra indicated that the main structure of glass did not change by the introduced $CeO_2$. But the optical band gap calculated by the absorption spectra indicated an increase of non-bridge oxygen, which is coincide with the analysis of optical basicity. All these changes of structure gave provides to the increased emission spectra. Finally, the transmittance of sample was higher than 75%, and the UV absorption edge moves toward the long wavelength less than 400 nm. The excitation and emission spectra of the glass samples determined that the optimal doping amount of $CeO_2$ is 0.6% (C4) which has the highest luminescence intensity with a short lifetime (25.55 ns). In summary, this $Ce^{3+}$ doped borosilicate glass material was expected to be the matrix material for the high sensitivity detection.

Response Letter is available for this paper at: http://cjl.lightpublishing.cn/thesisDetails#10.37188/CJL.20230209.

**References:**


[1] 姜代武, 宋博, 杨旭, 等. $Tb^{3+}$掺杂硅酸盐闪烁玻璃发光特性[J]. 发光学报, 2009, 30(3): 363-367.
JIANG D W, SONG B, YANG X, *et al*. Luminescent property of $Tb^{3+}$ doped silicate scintillating glass [J]. *Chin. J. Lumin.*, 2009, 30(3): 363-367. (in Chinese)

[2] ZHANG J, XIANG Y D, WANG C, *et al*. Recent advances in optical fiber enabled radiation sensors [J]. *Sensors*, 2022, 22(3): 1126.

[3] 黄立辉, 赵静涛, 赵士龙, 等. $Eu^{3+}$掺杂含$CaF_2$纳米晶锗酸盐微晶玻璃的制备及其发光性质[J]. 发光学报, 2020, 41(10): 1234-1240.
HUANG L H, ZHAO J T, ZHAO S L, *et al*. Preparation and luminescence properties of $Eu^{3+}$ doped germanate glass ceramics containing $CaF_2$ nanocrystals [J]. *Chin. J. Lumin.*, 2020, 41(10): 1234-1240. (in Chinese)

[4] 孙心瑗, 邓昌滨, 温玉锋, 等. $Eu^{3+}$激活氟氧硼酸锗酸盐闪烁玻璃的发光性能[J]. 发光学报, 2020, 41(4): 371-378.
SUN X Y, DENG C B, WEN Y F, *et al*. Luminescent properties of $Eu^{3+}$-activated oxyfluoride borogermanate scintillating glasses [J]. *Chin. J. Lumin.*, 2020, 41(4): 371-378. (in Chinese)

[5] HUANG L, WEI Z S, LUAN J Z, *et al*. Dual-core Ce:YAG-derived silicate scintillation fiber for real-time X-ray detection [J]. *J. Lightwave Technol.*, 2023, 41(20): 6577-6585.

[6] TOYAMA S, MATSUYAMA S, MIWA M, *et al*. Outer layer scintillating fiber for low-energy β-ray detection [J]. *Rev. Sci. Instrum.*, 2022, 93(11): 113106.

[7] 王欣欣, 黄立辉, 赵士龙, 等. $Tb^{3+}$掺杂高密度锗酸盐闪烁玻璃的发光性质[J]. 发光学报, 2018, 39(2): 115-120.
WANG X X, HUANG L H, ZHAO S L, *et al*. Luminescence properties of $Tb^{3+}$ doped high density germanate scintillating glasses [J]. *Chin. J. Lumin.*, 2018, 39(2): 115-120. (in Chinese)

[8] LIU J Q, ZHAO X D, XU Y S, *et al*. All-inorganic glass scintillators: scintillation mechanism, materials, and applications [J]. *Laser Photonics Rev.*, 2023, 17(7): 2300006.

[9] HU C Y, HUANG Y, DENG C L, *et al*. An innovative fluorescent fiber sensor based on Ce/Tb co-doped silica fiber for partial discharge detection [J]. *IEEE Sens. J.*, 2023, 23(7): 6939-6947.

[10] TILLMAN I J, DETTMANN M A, HERRING V, *et al*. High-density scintillating glasses for a proton imaging detector

[J]. *Opt. Mater.*, 2017, 68: 58-62.

[11] RITTISUT W, WANTANA N, BUTBUREE A, *et al.* Luminescence properties of $Ce^{3+}$-doped borate scintillating glass for new radiation detection material [J]. *Radiat. Phys. Chem.*, 2021, 185: 109498.

[12] LI W H, SUI Z X, FAN C L, *et al.* Intense radioluminescence from transparent $CsGd_2F_7$:$Ce^{3+}$ nano-glass scintillator [J]. *J. Eur. Ceram. Soc.*, 2023, 43(14): 6331-6336.

[13] WANG L, LU F M, LI X M, *et al.* A novel scintillating material based on $Cu^{+}$ doped borate glass [J]. *J. Lumin.*, 2023, 257: 119751.

[14] CHO J Y, LEE D H, JEONG D W, *et al.* Luminescence properties of $Dy^{3+}$ doped germanosilicate glass scintillator using proton beam [J]. *J. Korean Phys. Soc.*, 2023, 83(3): 168-171.

[15] 张勇, 吕景文, 韩冰, 等. $Ce^{3+}$和$Tb^{3+}$掺杂钆-钡-硅酸盐闪烁玻璃的发光性能 [J]. 发光学报, 2017, 38(1): 37-44.
ZHANG Y, LYU J W, HAN B, *et al.* Luminescence properties of $Ce^{3+}$ and $Tb^{3+}$ doped Gd-Ba-silicate scintillating glass [J]. *Chin. J. Lumin.*, 2017, 38(1): 37-44. (in Chinese)

[16] KAWANO N, OKAZAKI K, TAKEBUCHI Y, *et al.* Scintillation properties of $Er^{3+}$-activated BaO-$Nb_2O_5$-$TeO_2$ glasses [J]. *Jpn. J. Appl. Phys.*, 2023, 62(7): 072002.

[17] ZHANG Z J, YANG W. Effect of proton irradiation on the structure and luminescence properties of $Ce^{3+}$ doped lithium-borophosphate glasses [J]. *Opt. Mater. Express*, 2017, 7(11): 3979-3989.

[18] CHEN Q M, DING J X, YAO G P, *et al.* Spectroscopic properties of $Ce^{3+}$/$Tb^{3+}$ co-doped high silica scintillating glass [J]. J. *Non-Cryst. Solids*, 2017, 473: 54-58.

[19] SU M L, ZAHNG Q, GAO Y J, *et al.* Enhanced luminescence of $CsPbBr_3$ nanocrystals-glass composite scintillators based on $Ce^{3+}$-doped borosilicate glass [J]. *J. Lumin.*, 2022, 242: 118553.

[20] JIAO Y, SHAO C Y, GUO M T, *et al.* Influence of $Ce^{3+}$ ion on optical properties and radiation resistance in $Ce^{3+}$/$Tm^{3+}$-co-doped alumino-silicate glasses [J]. *Opt. Mater.*: X, 2022, 13: 100113.

[21] ZUO C, XIAO A, ZHOU Z, *et al.* Spectroscopic properties of $Ce^{3+}$ doped BaO-$Gd_2O_3$-$Al_2O_3$-$B_2O_3$-$SiO_2$ glasses [J]. J. *Non-Cryst. Solids*, 2016, 452: 35-39.

[22] INTACHAI N, WANTANA N, KAEWJAENG S, *et al.* Effect of $Gd_2O_3$ on radiation shielding, physical and optical properties of sodium borosilicate glass system [J]. *Radiat. Phys. Chem.*, 2022, 199: 110361.

[23] MHAREB M H A, ALAJERAMI Y S M, SAYYED M I, *et al.* Radiation shielding, structural, physical, and optical properties for a series of borosilicate glass [J]. J. *Non-Cryst. Solids*, 2020, 550: 120360.

[24] WANG J, BROCKLESBY W S, LINCOLN J R, *et al.* Local structures of rare-earth ions in glasses: the 'crystal-chemistry' approach [J]. J. *Non-Cryst. Solids*, 1993, 163(3): 261-267.

[25] RAJARAMAKRISHNA R, KAEWJAENG S, KAEWKHAO J, *et al.* Investigation of XANES study and energy transport phenomenon of $Gd^{3+}$ to $Ce^{3+}$ in CaO-$SiO_2$-$B_2O_3$ glasses [J]. *Opt. Mater.*, 2020, 102: 109826.

[26] LUO W, BAO Z H, JIANG W H, *et al.* Effect of $B_2O_3$ on the crystallization, structure and properties of MgO-$Al_2O_3$-$SiO_2$ glass-ceramics [J]. *Ceram. Int.*, 2019, 45(18): 24750-24756.

[27] WU D Q, ZHU C F, ZHANG M M. $Ce^{3+}$-and $Dy^{3+}$-doped oxyfluoride borosilicate glasses with near white luminescence [J]. *J. Am. Ceram. Soc.*, 2016, 99(5): 1587-1593.

[28] EL-DAMRAWI G, EL-EGILI K. Characterization of novel $CeO_2$-$B_2O_3$ glasses, structure and properties [J]. *Phys.* B: *Condens. Matter*, 2001, 299(1-2): 180-186.

[29] YANG Y B, WU L, TENG Y C, *et al.* Effect of ZnO content on microstructure, crystallization behavior, and thermal properties of $x$ZnO-30$B_2O_3$-(65−$x$)$Bi_2O_3$-5BaO glass [J]. J. *Non-Cryst. Solids*, 2019, 511: 29-35.

[30] LAORODPHAN N, POODDEE P, KIDKHUNTHOD P, *et al.* Boron and pentavalent vanadium local environments in binary vanadium borate glasses [J]. J. *Non-Cryst. Solids*, 2016, 453: 118-124.

[31] KAMITSOS E I, KARAKASSIDES M A, CHRYSSIKOS G D. Vibrational spectra of magnesium-sodium-borate glasses. 2. Raman and mid-infrared investigation of the network structure [J]. *J. Phys. Chem.*, 1987, 91(5): 1073-1079.

[32] INGO G M, PAPARAZZO E, BAGNARELLI O, *et al.* XPS studies on cerium, zirconium and yttrium valence states in plasma-sprayed coatings [J]. *Surf. Interface Anal.*, 1990, 16(1-12): 515-519.

[33] DAUSCHER A, HILAIRE L, LE NORMAND F, *et al.* Characterization by XPS and XAS of supported Pt/$TiO_2$-$CeO_2$ catalysts [J]. *Surf. Interface Anal.*, 1990, 16(1-12): 341-346.

[34] YU H F, XIN R, ZHANG X Q, *et al*. Crystallization behavior, quantitation of $Ce^{3+}/Ce^{4+}$ and chemical stability analysis of multiple alkaline earths borosilicate glasses for immobilizing simulated tetravalent actinides [J]. J. *Non-Cryst. Solids*, 2021, 558: 120642.

[35] SUN X Y, XIAO Z H, WU Y T, *et al*. Fast $Ce^{3+}$-activated borosilicate glass scintillators prepared in air atmosphere [J]. *Ceram. Int.*, 2017, 43(3): 3401-3404.

[36] CHEN Y P, LUO D L, LUO L Z, *et al*. Luminescence of $Ce^{3+}/Tb^{3+}$ ions in lithium-magnesium aluminosilicate glasses [J]. J. *Non-Cryst. Solids*, 2014, 386: 124-128.

[37] REISFELD R, MINTI H, PATRA A, *et al*. Spectroscopic properties of cerium in glasses and their comparison with crystals [J]. *Spectrochim. Acta Part* A: *Mol. Biomol. Spectrosc*, 1998, 54(13): 2143-2150.

[38] TAUC J, MENTH A. States in the gap [J]. J. *Non-Cryst. Solids*, 1972, 8-10: 569-585.

[39] WANTANA N, RUANGTAWEEP Y, KAEWNUAM E, *et al*. Strong emission from $Ce^{3+}$ doped gadolinium oxyfluoroborate scintillation glasses matrix [J]. *Radiat. Phys. Chem.*, 2021, 185: 109497.

[40] YOUSEF E S, EL-ADAWY A, KOSHKHANY NEL, *et al*. Optical and acoustic properties of $TeO_2/WO_3$ glasses with small amount of additive $ZrO_2$ [J]. *J. Phys. Chem. Solids*, 2006, 67(8): 1649-1655.

[41] CHEWPRADITKUL W, HE X, CHEN D, *et al*. Luminescence and scintillation of $Ce^{3+}$-doped oxide glass with high $Gd_2O_3$ concentration [J]. *Phys. Status Solidi*(a), 2011, 208(12): 2830-2832.

[42] PENG M Y, DONG G P, WONDRACZEK L, *et al*. Discussion on the origin of NIR emission from Bi-doped materials [J]. J. *Non-Cryst. Solids*, 2011, 357(11-13): 2241-2245.

[43] CHUNG J, INOUE H, YOSHIMOTO K, *et al*. Optical properties of novel oxyfluoride glasses on the systems of $LaF_3$-$LaO_{3/2}$-$NbO_{5/2}$ and $LaF_3$-$LaO_{3/2}$-$NbO_{5/2}$-$AlO_{3/2}$ [J]. *J. Am. Ceram. Soc.*, 2021, 104(8): 3963-3972.

[44] 刘力挽, 周秦岭, 邵冲云, 等. $Ce^{3+}$掺杂$SiO_2$-$Al_2O_3$-$Gd_2O_3$玻璃的闪烁性能 [J]. *物理学报*, 2015, 64(16): 167802.
LIU L W, ZHOU Q L, SHAO C Y, *et al*. Scintillation properties of $Ce^{3+}$ doped $SiO_2$-$Al_2O_3$-$Gd_2O_3$ glass [J]. *Acta Phys. Sinica*, 2015, 64(16): 167802. (in Chinese)

[45] PAN L Y, DAGUANO J K M F, TRINDADE N M, *et al*. Scintillation, luminescence and optical properties of Ce-doped borosilicate glasses [J]. *Opt. Mater.*, 2020, 104: 109847.

[46] WANG Q, YANG B, ZHANG Y P, *et al*. High light yield $Ce^{3+}$-doped dense scintillating glasses [J]. *J. Alloys Compd.*, 2013, 581: 801-804.

[47] PARK J M, HA D H, KAEWJEANG S, *et al*. Luminescence properties of $Ce^{3+}$ doped gadolinium-calcium-silicaborate glass scintillator [J]. *Radiat. Meas.*, 2016, 99: 166-169.

**张芳铭**(1998-),女,吉林松原人,硕士,2023年于长春理工大学获得硕士学位,主要从事特种玻璃材料的研究。
E-mail: zhangfangming0517@163.com

**郭艳艳**(1987-),女,河南南阳人,博士,副教授,硕士生导师,2013年于中国科学院上海光学精密机械研究所获得博士学位,主要从事特种光学玻璃与光纤材料的研究。
E-mail: guoyanyan@cust.edu.cn